RSC Advances

ROYAL SOCIETY OF CHEMISTRY

www.rsc.org/advances

Journal Name

ARTICLE

HfO_2 Nanodots Incorporated in TiO_2 and its hydrogenation for High Performance Dye Sensitized Solar Cells

Received 00th January 20xx,
Accepted 00th January 20xx

DOI: 10.1039/x0xx00000x

www.rsc.org/

Devika Laishram, Kiran P. Shejale, Rakesh K. Sharma* and Ritu Gupta*

Black titania (H-TiO_2) as a photoanode material has attracted huge attention due to its extremely high optical absorption in the visible region. Herein, black TiO_2 doped with HfO_2 is demonstrated to possess ~ 45.7 % higher photo-conversion efficiency than H-TiO_2 under identically similar conditions. The incorporation of HfO_2 nanodots increase the optical scattering in H-TiO_2 only when it itself undergoes hydrogenation along with TiO_2. Hafnia doped TiO_2 (HfO_2/TiO_2) is synthesized by a combination of simple sol-gel and hydrothermal method followed by thermal annealing under controlled hydrogen atmosphere. The hydrogenated H-(TiO_2/HfO_2) is found to exhibit very high optical absorption, however, slightly lower than H-TiO_2 due to light scattering by HfO_2 nanodots. We observe a sharp decrease in optical band gap of TiO_2/HfO_2 from 3.2 to 2.4 eV up on hydrogen annealing which is important in solar applications as demonstrated with the fabrication of high efficiency dye sensitized solar cell (DSSC).

1. Introduction

Energy harvesting via sun is a global challenge that require efficient and robust solar active materials. Solar applications involving photoactive material such as photocatalytic studies,[1] solar cells[2] and hydrogen production,[3] have lately attracted significant attention due to increasing energy demand and depleting non-renewable resources of energy. Titania (TiO_2) being lower in cost and easily available, is an exemplary photoanode material used in dye sensitized solar cells (DSSC). The performance of DSSC depends on the trade-off between light harvesting efficiency and charge collection across the photoanode. Much of the contemporary research focuses around tailoring the properties of TiO_2 by different approaches that include altering the morphology,[4,5] tuning the phase[6] or by external doping.[7,8] In order to increase the charge collection ability, TiO_2 is synthesized in one-dimensional morphologies such as nanorods and nanotubes, apart from mesospheres and nanospheres. Although, one-dimensional TiO_2 nanorods and nanotubes provide a highway for electron conduction, its surface area is still lower with regards to application in DSSC.[9,10,11] Particularly, TiO_2 mesospheres and nanospheres have good light scattering ability and high surface area for greater absorption of dye that maximizes the light harvesting capability of TiO_2 thereby increasing the photocurrent generation.[2,12]

Substantial efforts have been focussed on the phase tunable synthesis of TiO_2 for improving the charge recombination in TiO_2. For example, some of us synthesized TiO_2 at sub-zero temperatures with different percentage of anatase and rutile phases with increased solar cell efficiency of 8.6% for anatase dominated phase.[13] Recently, the TiO_2 with anatase phase synthesized with exposed {001} facet have exhibited improved performance in DSSC.[14] Another approach adopted for improving the optical properties of TiO_2 is by doping it with various metals,[8,15-17] non-metals[18-21] and metal oxides.[22-24] TiO_2 with a wide band gap of 3.0-3.2 eV, absorbs mainly in UV region (250-400 nm) which is only a part of entire solar spectrum. Thus, band gap engineering of TiO_2 is highly important for its effective utilization. For example, hydrogenation of TiO_2 lower its band gap from 3.2 to 1.8 eV and enhances the solar cell efficiency by 28%.[25] Doping in TiO_2 not only alters the bandgap but also helps in improving the charge transfer efficiency.[26] An exhaustive literature survey on doping of different metals, semiconductors and dielectrics in TiO_2 is provided in ESI, Table S1. In case of dielectrics such as HfO_2, Al_2O_3 and ZrO_2, the surface of TiO_2 is usually modified with a layer of dielectric material in the form of core-shell structure to curb the electron recombination process and also to decrease the electron injection resistance at the electrode-electrolyte interface for the improvement of DSSC.[22,27-31] However, the role of HfO_2 as dopant in TiO_2 nanosphere have not been explored previously. The electronic shell of Hf in HfO_2 ($[Xe]4f^{14}5d^26s^2$) is loosely bound to the nucleus that can possibly contribute electrons to TiO_2 for improved conduction. Moreover, HfO_2 having high coordination sphere can offer high

Department of Chemistry, Indian Institute of Technology Jodhpur, Jodhpur, Rajasthan, India. 342011.
*Corresponding Author: Dr. Ritu Gupta (ritu@iitj.ac.in); Dr. Rakesh K. Sharma (rks@iitj.ac.in)

Electronic Supplementary Information (ESI) available: Table S1: literature survey of doping in TiO_2, Fig. S1: FESEM images of HfO_2 doped TiO_2, Fig. S2: BET Surface area measurements of HfO_2/TiO_2 and TiO_2; Fig. S3: XRD pattern, Fig. S4: TEM images of H-TiO_2, Fig. S5: Raman spectra of H-HfO_2/TiO_2 and H-TiO_2, Fig. S6: Schematic of DSSC, Fig. S7 BET surface area measurements; Fig. S8 Dye deloading calculation using absorption spectrum, Table S2: EIS performance parameters calculation.

surface area and its dielectric nature can contribute towards enhanced optical absorption. Interestingly, the hydrogenation of HfO_2 is known to lower its resistance state that can be utilized in synergy with hydrogenated TiO_2. Thus, in this study, TiO_2 with finely distributed HfO_2 nanodots is synthesized by hydrothermal method and hydrogenated. The H-HfO_2/TiO_2 is compared with H-TiO_2 as a photoanode material and several devices have been fabricated. This work emphasizes on the feasibility of doping a high coordination sphere dielectric such as HfO_2 along with its hydrogenation resulting in enhanced properties of TiO_2 photoactive material in all solar applications. This is clearly illustrated by the enhancement in the efficiency of dye sensitized solar cell by 65% as compared to P25 TiO_2.

2. Experimental

2.1 Synthesis of hydrogenated HfO_2/TiO_2 and TiO_2

The samples of TiO_2, HfO_2/TiO_2, H-TiO_2 and H-HfO_2/TiO_2 nanospheres were firstly prepared via a slightly modified sol–gel hydrothermal method.[32] 70 mM titanium isopropoxide (TIP) and 4 mM hafnium propoxide (HIP) was added dropwise into mixture of 200 mL ethanol, 1.975 g hexadecylamine (HDA) under vigorous stirring. The mixture was kept undisturbed for 18 hrs to form a gel and then filtered using a vacuum filter followed by drying at room temperature. The 0.8 g of sample was dispersed in 10 mL ethanol, 5 mL deionised water and 0.25 mL liquor ammonia. The obtained mixture was transferred in a 20 mL Teflon-lined stainless steel autoclave and kept at 160 °C for 8 hrs in an oven. After the completion of reaction, the resultant product was washed three times with deionized water (DI) and absolute ethanol before drying in a vacuum oven at 70 °C overnight and subsequently calcined at 500 °C for 2 hrs to obtain HfO_2/TiO_2 nanospheres. Same recipe was repeated without any addition of HIP resulting in the synthesis of white powder of TiO_2 nanospheres. These were placed in the quartz boat and heated in tube furnace under a gas flow of 10% H_2 and 90% N_2 for 2 hrs at 500 °C, respectively. The hydrogen annealing of TiO_2, HfO_2/TiO_2 was performed at a heating rate of 2.5 °C min^{-1} under constant hydrogen flow resulting in H-TiO_2 and H-HfO_2/TiO_2 respectively.

2.2 DSSC fabrication

H-HfO_2/TiO_2 and TiO_2 (P25) powders were mixed in an optimized 4:6 ratio[13] for the preparation of photoanode film for which a paste was prepared by uniformly grinding and mixing these powders with ethyl cellulose in α-terpinol and ethanol (weight% ratio: 2.7:1:3.38). The paste was screen printed on the FTO substrates and dried at 120 °C for 6 min. The procedure of screen printing was repeated for five times to increase the layer thickness. The electrodes were sintered at 450 °C for 30 min in the air resulting in a film of ~10 µm thickness which was used as such for DSSC fabrication. Similar procedure was adopted for preparing H-TiO_2 photoanode film. The platinum sol was deposited onto the FTO glass substrates and then calcined at 450 °C for 30 min to obtain the platinum counter electrode. The photoanodes were soaked in N3 standard dye (0.5 mM) solution for 18 hrs and kept in dark. Finally, the soaked photoanodes along with Pt counter electrode were assembled using a Surlyn spacer resulting in a sandwich structure. Iodolyte Z50 from Solaronix was used as the electrolyte.

2.3 Characterization

TEM imaging was performed by transmission electron microscope (FEI Tecnai-G2 T20). For imaging, ~ 10 mg of sample was dispersed in ethanol and drop coated on a copper grid and allowed to dry before imaging. Diffuse reflectance spectra were recorded using UV-vis spectrophotometer (Varian Cary 4000) with PTFE (polytetrafluoroethylene) as the standard material for baseline correction. Specific surface area was analyzed by N_2-adsorption-desorption isotherm (Quantachrome autosorb iQ3). Raman spectra were recorded in the range of 100-1000 cm^{-1} using confocal Raman microscope (Renishaw, UK) with semiconductor diode laser excitation source (0.5% power) at an emission wavelength of 785 nm. Solar Simulator (model number SS50AA, Photoemission Tech) was used to illuminate the cell under AM 1.5G solar irradiation. Electrochemical workstation (CHI6600) was used for I-V measurements and EIS analysis. HRTEM images were analysed using ImageJ and gatan digital micrograph software.

3. Results and Discussion

The TiO_2 nanospheres doped with HfO_2 are synthesized following a slightly modified hydrothermal method as shown

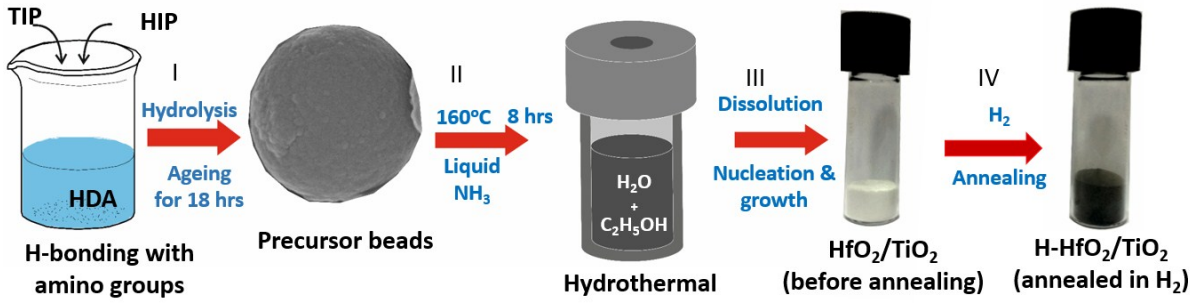

Figure 1 Schematic demonstrating the synthesis method for hydrogenated TiO_2 nanospheres doped with HfO_2 nanodots.

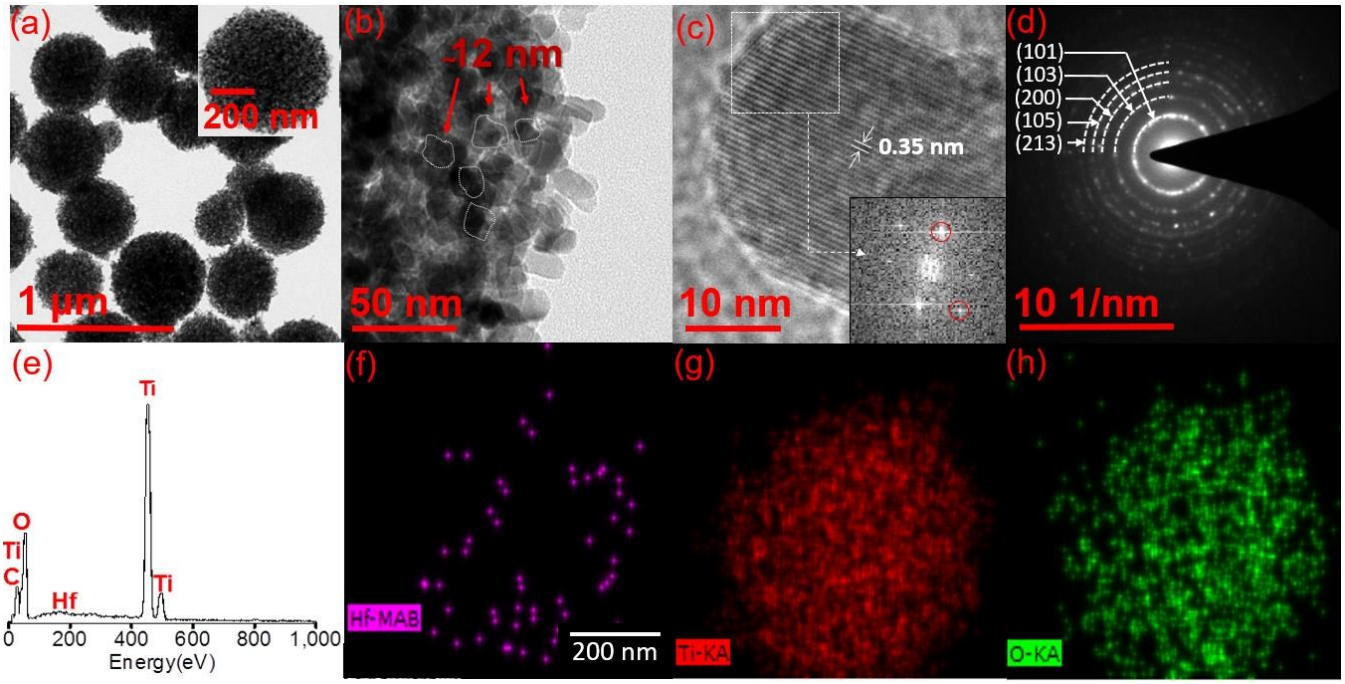

Figure 2 (a) TEM images of H-HfO_2/TiO_2 and (b) a highly magnified view of H-HfO_2/TiO_2 nanosphere. (c) High resolution TEM image and (d) SAED pattern of H-HfO_2/TiO_2. (e) EDS spectrum and (f-h) EDS maps corresponding to Hf M, Ti K and and O K signal respectively. Note that the signal C K in e originates from the carbon tape and can be neglected.

schematically in **Fig. 1**. Typically, titanium isopropoxide (TIP) precursor is hydrolysed in hexadecylamine (HDA) and aged for 18 hrs. The HDA-TiO_2 lamellar structures are usually formed upon hydrolysis of TIP. This composite tend to form micelles that polymerizes resulting in the formation of mesoporous inorganic TiO_2 nanospheres.[33] Upon addition of TIP to the alcoholic medium, the clear solution instantly turned milky white giving rise to phase-separated, highly-monodispersed spherical beads. This solution is taken as a precursor for hydrothermal reaction under conditions shown in step 2, leading to the formation of crystalline TiO_2 nanospheres. The TiO_2 powder is hydrogenated by annealing at 500° C for 2 hrs under H_2 atmosphere as seen by the discoloration from white to grey black. In this work, hydrogenated HfO_2 doped TiO_2 is prepared by introducing hafnium propoxide (HIP) as hafnia precursor along with TIP (starting titania precursor) in different atomic weight ratio of 1%, 5% and 10%) following the same steps as above (ESI, Fig. S1). The doping level of HfO_2 in TiO_2 is optimized to be minimum (1%) since it is an insulating dielectric material with low electron affinity of 2.5 eV. Importantly, the surface area of HfO_2/TiO_2 with 1% doping increases in comparison to TiO_2 as expected. (Fig. S2). The hydrogenated sample with 1% HfO_2 doped in TiO_2 was used for further studies.

The morphology and structural composition of H-HfO_2/TiO_2 were characterized as shown in **Fig. 2**. Due to low doping percentage of HfO_2, no significant change in peak position was observed in XRD pattern (ESI, Fig. S3). The TEM image in Fig. 2a indicates the formation of uniformly distributed nanospheres and is quite similar to that of H-TiO_2 (ESI, Fig. S4) The average diameter of a single nanosphere of H-HfO_2/TiO_2 is 470 ± 2 nm (Fig. 2a, inset). A nanosphere consisted of crystallites of size ~12 nm (Fig. 2b). The HRTEM image shows the lattice spacing of 0.35 nm corresponding to (101) plane of TiO_2 anatase (Fig. 2c). The marked area at the edge of particle exhibited Moiré pattern which was carefully examined by FFT as shown in inset of **Fig. 2c**. The electron diffraction (ED) pattern exhibits concentric rings that are indexable to the lattice planes (101), (103), (200), (105) and (213) and corresponds to anatase phase of TiO_2 (Fig. 2d). The HfO_2 could not be identified in ED and

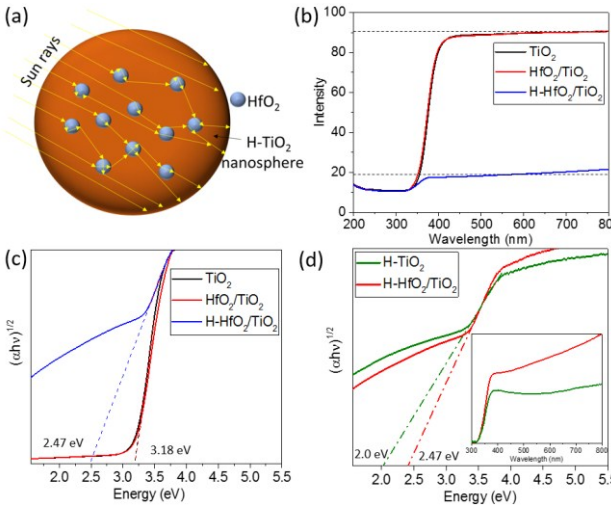

Figure 3 (a) Schematic demonstrating the light interaction with HfO_2 doped hydrogenated TiO_2 nanosphere. (b) UV-vis diffuse reflectance spectra and (c) Tauc plot of $(\alpha h\nu)^{1/2}$ versus energy for band gap calculation of TiO_2, HfO_2/TiO_2 and H-HfO_2/TiO_2. (d) $(\alpha h\nu)^{1/2}$ versus energy and reflectance spectra (inset) for H-TiO_2 and H-HfO_2/TiO_2.

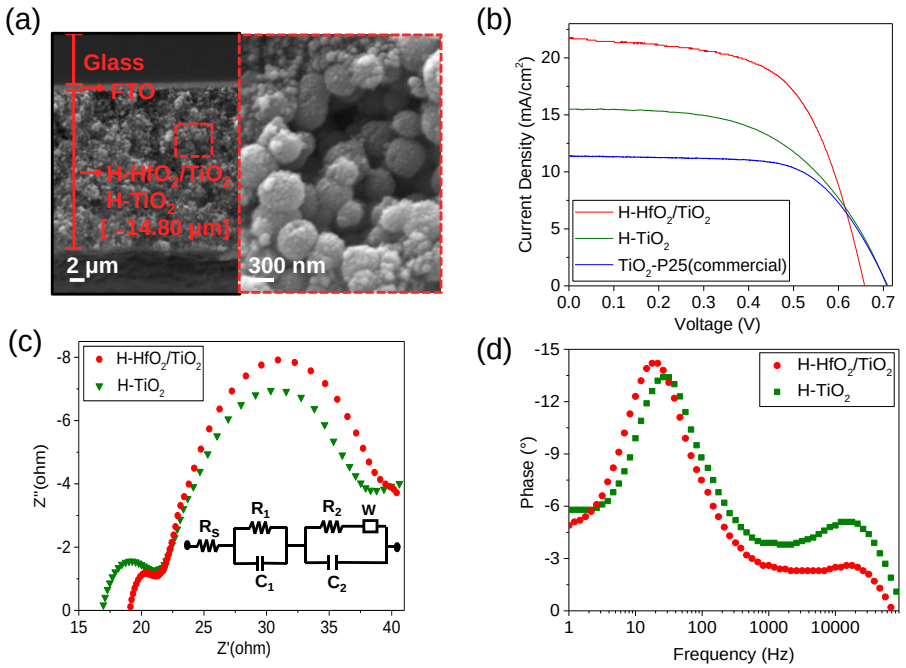

Figure 4 (a) Cross-sectional SEM image of the photoanode deposited on FTO along with its magnified image. Note that Au/Pd metal layer is sputtered on photoanode for improving the image contrast. (b) Current density and voltage (J-V) characteristics of the DSSC based on H-HfO_2/TiO_2 and H-TiO_2 along with P25 TiO_2 (c) Nyquist plot and (d) Bode plot for the DSSC based on H-HfO_2/TiO_2 and H-TiO_2. Inset of (c) is the equivalent circuit diagram used for fitting the curves.

HRTEM however, EDS spectrum shows signals corresponding to Hf M, Ti K and O L due to the presence of HfO_2 in TiO_2 (Fig. 2e). The EDS map of Hf in Fig. 2e shows nanodots in the area enclosed by the TiO_2 nanosphere (Fig. 2f and 2g) which infers presence of ultrasmall but monodispersed HfO_2 nanodots in TiO_2. The doping of HfO_2 nanodots as well as hydrogenation has direct influence on the optical properties of TiO_2. As shown schematically in **Fig. 3a**, the optical path length is increased by the introduction of HfO_2 nanodots in TiO_2 resulting in higher scattering. **Fig. 3b** and **3c** shows the optical reflection spectra and corresponding band gap for TiO_2 after doping with HfO_2 and upon hydrogenation. The incorporation of HfO_2 nanodots in small quantities (1 %) has little influence on the optical absorption and in turn, the optical band gap of TiO_2 (3.18 eV) as shown in Figure 3b. To extend the optical absorption in the visible region, the HfO_2/TiO_2 is annealed in hydrogen as shown in **Fig. 1** (step IV). Hydrogen annealing of TiO_2 is known to extend its light absorption towards visible region due to formation of sub band gap states between the conduction and valence bands with the formation of oxygen vacancy sites.[34] The generation of defects lead to lattice disorientation.[1,35-37] However, hydrogenation of HfO_2 in TiO_2 is not very well studied. The UV-vis diffuse reflection spectrum of HfO_2/TiO_2 is flat and featureless in the visible (400-800 nm) region, however, the reflection decreases drastically upon hydrogenation as shown in Fig. 3b. The decrease is more than the hydrogenated TiO_2 indicating clear hydrogenation of HfO_2 as well. In case of TiO_2, band gap is known to decrease upon hydrogenation due to the presence of oxygen vacancies and Ti^{3+} sites in the crystal structure.[38] Similarly, the optical band gap of the HfO_2/TiO_2 decreases from ~3.18 to ~2.4 eV upon hydrogenation (Fig. 3c). The effect of HfO_2 doping on band gap is negligible under air annealed conditions, however, it is clearly visible in hydrogenated samples (Fig. 3d). Due to the high coordination sphere of HfO_2, the defect density in H-HfO_2/TiO_2 increases as shown by the Raman spectra (Fig. S5). There is a shift in the stretching mode of Eg peak from 146 to 151 cm^{-1} due to the induced defects and possible disorientation in the lattice structure upon hydrogenation of HfO_2 in TiO_2. The optical reflection for H-HfO_2/TiO_2 in comparison to TiO_2 (inset, Fig. 3d) is remarkably lowered possibly due to increased optical scattering by hydrogenated HfO_2 resulting in a lowered band gap of 2.4 eV. However, in comparison to H-TiO_2 (2.0 eV), the bandgap for H-HfO_2/TiO_2 is still lower which might be important for enhancement in the visible light absorption for solar cell application.

The cross-sectional view of the DSSC fabricated using H-HfO_2/TiO_2 nanospheres is shown in **Fig. 4a**. It represents the layer-by-layer arrangement of the photoanode to be used in fabrication of DSSC. The magnified SEM image at the cross-section is slightly uneven at the edge (Fig. 4a; right) however in-depth focus shows the tightly packed morphology of the deposited film. A schematic of complete sandwich structure of DSSC is shown in Fig. S6. **Fig. 4b** shows the J-V characteristics of DSSC based on H-HfO_2/TiO_2, H-TiO_2 and P25 TiO_2. The corresponding photovoltaic parameters are detailed in Table 1. The H-HfO_2/TiO_2 photoanode based DSSC has strikingly higher current density, J_{SC} of 21.74 mA/cm^2 with nominal V_{OC} of 0.66 V in comparison to H-TiO_2. As seen from the data, the H-HfO_2/TiO_2 based DSSC exhibits enhanced photo-conversion efficiency of 8.6% while H-TiO_2 and P25 TiO_2 show 5.9% and 5.2% efficiency values under similar conditions. This is an intriguing result and probably occurs due to enhanced light absorption (discussed in Fig. 3), higher surface area (Fig. S7)

Table 1 Photovoltaic performance parameters of the DSSC based on H-HfO_2/TiO_2 and H-TiO_2.[a]

Cell	J_{SC} (mA/cm^2)	V_{OC} (V)	FF	η (%)
H-HfO_2/TiO_2	21.74±0.4	0.66±0.1	60.2±0.08	8.6±0.1
H-TiO_2	15.49±0.1	0.71±0.04	53.97±0.07	5.9±0.9
TiO_2- P25	11.4.±0.01	0.71±0.01	64.6±0.01	5.2±0.08

a The results represent relative data of many experimental readings averaged over 3 cells.

and lower recombination rate. From BET measurements in Fig. S8, surface area of H-HfO_2/TiO_2 is calculated to be higher (74.21m^2/g) as compared to H-TiO_2 (56.186 m^2/g). The surface area effect was studied by calculating the amount of dye loaded on the photoanode and deloading it using NaOH solution. It was observed that the H-HfO_2/TiO_2 photoanode relatively soaked 35% more dye than the H-TiO_2. The detailed calculation along with the absorbance diagram is given in ESI, Fig. S7. This clearly brings out the fact that H-HfO_2/TiO_2 offers higher surface area thus contributing to the increased efficiency.

Electrochemical impedance spectroscopy (EIS) measurements were performed for the DSSCs based on H-HfO_2/TiO_2 and H-TiO_2 in the frequency range between 1 to 10^5 Hz under 1 sun illumination for understanding the electron recombination and interfacial charge transfer processes. The Nyquist plots in **Fig. 4c** show three semicircles in the complex plane that represent the interface resistances between the photoanode and electrolyte. The plots are fitted with an equivalent circuit consisting of a series resistance (R_S), Pt-electrolyte capacitance, a charge transfer resistance in the counter electrode and the electrolyte interface (R_1 and R_2) and a Warburg resistance, W, due to ion transfer in the electrolyte.[39,40] The parameters R_S, R_1, R_2 and W are listed in Table S2. The impedance Bode phase plots in **Fig. 4d** display a frequency peak (ω_{max}) that corresponds to various charge transfer processes occurring in the DSSCs. The Bode plot for H-TiO_2 has ω_{max} shifted from 29.10 Hz to 19.54 Hz as a result of hydrogenation of HfO_2 in H-HfO_2/TiO_2. The ω_{max} is inversely related to the electron lifetime ($\tau_n=1/\omega_{max}$). A decrease in value of ω_{max} in DSSC based on H-HfO_2/TiO_2 indicates decrease in the charge recombination in comparison to H-TiO_2. The electron lifetime τ_n was calculated using the formula $\tau_n = (R_1*C_1)$ where R_1 and C_1 are the charge transfer resistance and chemical capacitance.[26] H-HfO_2/TiO_2 was found to have higher value of τ_n (0.142 ms) than H-TiO_2 (0.056 ms). This is a significant increase in the electron lifetime and this leads to reduction in charge recombination in the fabricated device. Thus, a longer electron lifetime (τ_n) and high value of R_1 for the H-HfO_2/TiO_2 based DSSC result in improved J_{SC} values. The effect of different HfO_2 loading and optimization of hydrogenation conditions will be carried out in future studies for further improving the performance of these devices.

4. Conclusions

In conclusion, hydrogenated TiO_2 doped with HfO_2 nanodots were prepared by combination of sol-gel and hydrothermal method. HfO_2 nanodots increases the defect density upon hydrogenation and shifts the optical absorption of H-HfO_2/TiO_2 from IR towards visible region. This is clearly seen from an increase in band gap from 2.03 eV to 2.4 eV. Due to increased surface area, there is a clear enhancement in dye uptake capability of H-HfO_2/TiO_2 (10.1×10^{-9} mol.cm^{-2}) as compared to H-TiO_2. The DSSC fabricated using H-HfO_2/TiO_2 with an optimal band gap of 2.4 eV exhibits an efficiency of 8.6% with a photocurrent density of 21.7 mA/cm^2. This may be attributed to the optical light trapping effects and enhanced surface area of TiO_2 with addition of HfO_2 nanodots and its hydrogenation.

5. Acknowledgements

The authors are grateful to Department of Science and Technology, Govt. of India and Indo-Portuguese Program of Cooperation in Science and Technology, 2014-2016 (Grant Number SR/FT/CS-144/2011 and INT/Portugal/PO2/2013) in terms of financial support. We would also like to acknowledge the Material Research Centre, MNIT Jaipur, India for TEM measurements and JNCASR, Bangalore, India for FESEM characterization.

6. References

1 W. Zhou, W. Li, J. Q. Wang, Y. Qu, Y. Yang, Y. Xie, K. Zhang, L. Wang, H. Fu and D. Zhao, *J. Am. Chem. Soc.*, 2014, **136**, 9280.
2 D. C. F. Sauvage, P. Comte, F. Huang, L.-P. Heiniger, Y.-B. Cheng, R. A. Caruso, M. Graetzel, *ACS Nano*, 2010, **4**, 6.
3 M. Ni, M. K. H. Leung, D. Y. C. Leung and K. Sumathy, *Renew. Sustainable Energy Rev.*, 2007, **11**, 401.
4 M. R. Subramaniam, S. Devanathan and D. Kumaresan, *RSC Adv.*, 2014, **4**, 36791.
5 G. Tian, Y. Chen, W. Zhou, K. Pan, C. Tian, X. R. Huang and H. Fu, *Cryst. Eng. Comm.*, 2011, **13**, 2994.
6 K. P. Shejale, D. Laishram, M. S. Roy, M. Kumar and R. K. Sharma, *Mater. Design*, 2016, **92**, 535.
7 A. Latini, C. Cavallo, F. K. Aldibaja, D. Gozzi, D. Carta, A. Corrias, L. Lazzarini and G. Salviati, *J. Phys. Chem. C*, 2013, **117**, 25276.
8 B. Roose, S. Pathak and U. Steiner, *Chem. Soc. Rev.*, 2015, **44**, 8326.
9 D. Song, P. Cui, T. Wang, B. Xie, Y. Jiang, M. Li, Y. Li, S. Du, Y. He, Z. Liu and J. M. Mbebgue, *Nano Energy*, 2016, **23**, 122.
10 M. J. Jeng, Y.L. Wung, L.-B. Chang and L. Chow, *Int. J. Photoenergy*, 2013, **2013**, 1.
11 Z. Wang, S. Ran, B. Liu, D. Chen and G. Shen, *Nanoscale*, 2012, **4**, 3350-3358.
12 Z. Q. Li, Y. P. Que, L. E. Mo, W. C. Chen, Y. Ding, Y. M. Ma, L. Jiang, L. H. Hu and S. Y. Dai, *ACS Appl. Mater. Interfaces*, 2015, **7**, 10928.
13 K. P. Shejale, D. Laishram and R. K. Sharma, *RSC Adv.*, 2016, **6**, 23459.
14 L. Chu, Z. Qin, J. Yang and X. Li, *Sci. Rep.*, 2015, **5**, 12143.
15 K. Karthik, S. K. Pandian and N. V. Jaya, *Appl. Surf. Sci.*, 2010, **256**, 6829.
16 K. H. Ko, Y. C. Lee and Y. J. Jung, *J. Colloid Interf. Sci.*, 2005, **283**, 482.
17 X. Zhang, S. T. Wang and Z.-S. Wang, *Appl. Phys. Lett.*, 2011, **99**, 113503.

18 N. Feng, A. Zheng, Q. Wang, P. Ren, X. Gao, S. B. Liu, Z. Shen, T. Chen and F. Deng, *J. Phys. Chem. C*, 2011, **115**, 2709.
19 E. Guo and L. Yin, *Phys. Chem. Chem. Phys.*, 2015, **17**, 563.
20 D. G. F. David, J. Guerreiro, M. V. S. D. Silva, M. V. C. Meira, P. Bargiela, J. S.D. Almeida, J. A. Freitas and A. F. D. Silva, *J. Cryst. Growth*, 2012, **350**, 11.
21 X. Yu, B. Kim and Y. K. Kim, *ACS Catal.*, 2013, **3**, 2479.
22 P. Ramasamy, M. S. Kang, H. J. Cha and J. Kim, *Mater. Res. Bull.*, 2013, **48**, 79.
23 B. Kılıç, N. Gedik, S. P. Mucur, A. S. Hergul and E. Gür, *Mater. Sci. Semicond. Process*, 2015, **31**, 363.
24 S. Swetha and R. G. Balakrishna, *Chinese J. Catal.*, 2011, **32**, 789.
25 T. Su, Y. Yang, Y. Na, R. Fan, L. Li, L. Wei, B. Yang and W. Cao, *ACS Appl. Mater. Interfaces*, 2015, **7**, 3754.
26 S. P. Lim, A. Pandikumar, H. N. Lim, R. Ramaraj and N. M. Huang, *Sci. Rep.*, 2015, **5**, 11922.
27 L. Li, C. Xu, Y. Zhao, S. Chen and K. J. Ziegler, *ACS Appl. Mater. Interfaces*, 2015, **7**, 12824.
28 K. Manoharan, N. G. Joby and P. Venkatachalam, *Ionics*, 2014, **20**, 887.
29 H. J. Ahn, S. I. Kim, J. C. Yoon, J. S. Lee and J. H. Jang, *Nanoscale*, 2012, **4**, 4464.
30 J. E. Nam, H. J. Jo, D. H. Son, D. H. Kim and J. K. Kang, *Appl. Mech. Mater.*, 2014, **705**, 320.
31 M. Fadel, O. A. A. M, O.A. Omer, R.R. Basily, *Appl. Phys. A – Mater.*, 1998, **66**, 9.
32 L. C. D. Chen, F. Huang, P. Imperia, Y.-B. Cheng and R. A. Caruso, *J. Am. Chem. Soc.*, 2010, **132**, 7.
33 D. Chen, F. Huang, Y. B. Cheng and R. A. Caruso, *Adv. Mater.*, 2009, **21**, 2206.
34 A. Sinhamahapatra, J. P. Jeon and J. S. Yu, *Energ. Environ. Sci.*, 2015, **8**, 3539.
35 T. Leshuk, R. Parviz, P. Everett, H. Krishnakumar, R. A. Varin and F. Gu, *ACS Appl. Mater. Interfaces*, 2013, **5**, 1892.
36 Z. Wang, C. Yang, T. Lin, H. Yin, P. Chen, D. Wan, F. Xu, F. Huang, J. Lin, X. Xie and M. Jiang, *Energ. Environ. Sci.*, 2013, **6**, 3007.
37 L. L. X. Chen, P. Y. Yu and S. S. Mao, *Science*, 2011, **331**, 5.
38 G. Panomsuwan, A. Watthanaphanit, T. Ishizaki and N. Saito, *Phys. Chem. Chem. Phys.*, 2015, **17**, 13794.
39 P. Teesetsopon, S. Kumar, J. Dutta, *Int. J. Electrochem Sc.*, 2012, **7**, 12.
40 S. Sarker, A. J. S. Ahammad, H. W. Seo and D. M. Kim, *Int. J. Photoenergy*, 2014, **2014**, 1.

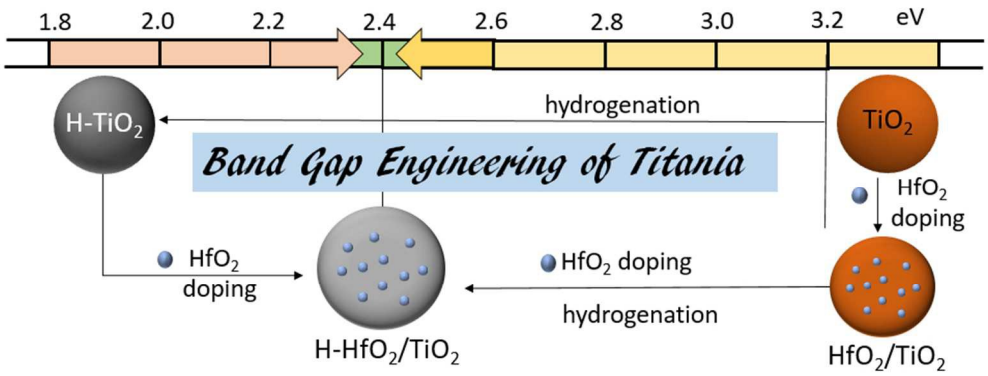

255x99mm (96 x 96 DPI)